A Single Nucleobase Tunes Nonradiative Decay in a DNA-Bound Silver Cluster

Yuyuan Zhang,[a] Chen He,[b] Kimberly de La Harpe,[c] Peter M. Goodwin,[d] Jeffrey T. Petty,[b,*] and Bern Kohler [a,*]

[a] Department of Chemistry and Biochemistry, The Ohio State University, 100 West 18th Avenue, Columbus, Ohio 43210, United States

[b] Department of Chemistry, Furman University, Greenville, South Carolina 29613, United States

[c] Department of Physics, United States Air Force Academy, U.S. Air Force Academy, Colorado 80840, United States

[d] Center for Integrated Nanotechnologies, Los Alamos National Laboratory, Mail Stop K771, Los Alamos, New Mexico 87545, United States

*Corresponding Authors:

Jeffrey T. Petty: jeff.petty@furman.edu, Tel: +1 864-294-2689

Bern Kohler: kohler.40@osu.edu, Tel: +1 614-688-2635

ABSTRACT: DNA strands are polymeric ligands that both protect and tune molecularly-sized silver cluster chromophores. We studied single-stranded DNA $C_4AC_4TC_3XT_4$ with X = guanosine and inosine that form a green fluorescent Ag_{10}^{6+}, but these two hosts are distinguished by their binding sites for and the brightness of their Ag_{10}^{6+} adducts. The nucleobase subunits in these oligomers collectively coordinate this cluster, and fs time-resolved infrared spectra previously identified one point of contact between the C2-NH_2 of the X = guanosine, an interaction that is precluded for inosine. Furthermore, this single nucleobase controls the cluster fluorescence, as the X = guanosine complex is ~2.5× dimmer. We discuss the electronic relaxation in these two complexes using transient absorption spectroscopy in the time window 200 fs – 400 μs. Three prominent features emerged: a ground state bleach, an excited state absorption, and stimulated emission. Stimulated emission at the earliest delay time (200 fs) suggests that the emissive state is populated promptly following photoexcitation. Concurrently, the excited state decays and the ground state recovers, and these changes are ~2× faster for the X = guanosine compared to the X = inosine cluster, paralleling their brightness difference. In contrast to similar radiative decay rates, the nonradiative rate is 7× higher with the X=guanosine vs inosine strand. A minor decay channel via a dark state is discussed. The possible correlation between the nonradiative decay and selective coordination with the X = guanosine/inosine suggests that specific nucleobase subunits with a polymeric DNA can modulate cluster-ligand interactions and in turn cluster brightness.

I. INTRODUCTION

Molecularly-sized and nanoscale silver clusters are more akin to organic dyes than to the bulk metal.[1-3] Due to their small sizes with sparsely–organized valence electronic states, they fluoresce across the optical and near-infrared spectral regions, and this emission can be reversibly toggled between bright and dark levels.[4-9] They are typically synthesized by reducing an ionic silver salt, and a nascent cluster can be quickly engulfed by using ligands to coordinate its surface and arrest growth.[10, 11] These ligands not only chemically trap but also control the fluorescence of their sequestered clusters.[12] A network of metal-ligand and peripheral intermolecular bonds incarcerate a cluster and can thereby tune the cluster's electronic states.[13, 14] Ligands can be further organized by covalently linking them together, and we focus on polymeric ligands that coordinate a cluster as a single unit.[15-18]

Single-stranded oligonucleotides are monodisperse polymers that coordinate molecular silver clusters through their nucleobase subunits.[19-21] The four canonical nucleobases have different binding sites and distinct affinities for silver, so their linear sequence along the DNA backbone establishes a specific ligation pattern.[22-24] Furthermore, the strand is able to fold and assemble around a cluster core because its anchoring backbone is flexible.[25-27] Thus, the sequence and structure of a DNA polymer establishes a unique binding site for a fluorescent silver cluster. Detailed maps of the coordination sites are emerging through visible and X-ray spectroscopy, mass spectrometry, X-ray crystallography, molecular modeling, and hydrodynamic studies.[22, 28-35]

Our studies are motivated by recent time-resolved infrared spectroscopy studies of the $C_4AC_4TC_3XT_4$–Ag_{10}^{6+} with X = guanosine and inosine. These clusters have matching optical spectra, as well as stoichiometries and charges (Figures S1 and S2, respectively) but are distinguished via their transient infrared spectra.[36] When the Ag_{10}^{6+} adduct was selectively photoexcited, the mid-infrared vibrations of the ligated X = guanosine and inosine were perturbed along with cytosines. This is a remarkable selectivity for one of the 18 nucleobases in the strand given that this single substitution results in indistinguishable steady-state FTIR spectra. These findings suggest coordination by the C_2-NH_2 of guanosine that is absent for the analogous C_2-H of inosine. The significance of this amino group is further bolstered because the Ag_{10}^{6+} cluster with the X = guanosine vs. inosine strand is 2.5× dimmer.[27]

When DNA-silver cluster fluorophores are photoexcited, they can electronically relax through multiple channels on distinct time scales such as internal conversion to the ground state (< 1 ps), emission (< 10 ns), and crossing to/from a metastable dark state (< 100 μs).[37, 38] In the present studies, we follow both radiative and nonradiative relaxation from the emissive state in $C_4AC_4TC_3XT_4$-Ag_{10}^{6+} over a 9 decade time range via femtosecond and nanosecond transient absorption (fs- and ns-TA) spectroscopies. We combine observations from these transient absorption spectra along with time-resolved emission and fluorescence correlation spectroscopy studies to identify the key electronic states and relaxation pathways of the photoexcited Ag_{10}^{6+} cluster.

II. EXPERIMENTAL

The DNA-bound silver clusters were synthesized as described previously (see Supplementary Material for full discussion).[39] Ag_{10}^{6+} is the only molecularly-sized, partially-reduced adduct in the mass spectra, and spectroscopic studies suggest that it preferentially forms.[39]

fs-TA experiments in the 200 fs – 3.5 ns range probed electronic transitions in the UV-visible-NIR region for the DNA-AgC samples (~25 μM DNA-AgC recirculating in a 1 mm path length cell) (see Supplementary Material for full discussion). The sample was excited with ~140 fs laser pulses with a center wavelength of 490 nm. A low pump fluence of 0.03 mJ cm^{-2}, corresponding to an average of 0.02 excitons per cluster, was used to minimize degradation and to avoid multiphoton absorption (see Figure S3 and associated text in the Supplementary Material). In addition, the low pump fluence allows ground state bleach recovery kinetics to be recorded by minimizing scattered pump light. The instrument response time is approximately 200 fs (Figure S4). At t > 200 fs, the composite fs-TA spectra of both AgCs have similar positive and negative transient absorption bands (Figures 1a,b). fs-TA signals could not be detected in either sample at longer NIR wavelengths (λ_{probe} = 1000 – 1350 nm). Nanosecond transient absorption (ns-TA) experiments were performed using a nanosecond laser with a pulse width of 3 to 5 ns, and a Xe arc lamp (see Supplementary Material for full discussion) to observe slower relaxation pathways for the electronically excited clusters. The instrument response function is approximately 7 ns.

III. RESULTS AND DISCUSSION

2.1 Short Time Range

fs-TA spectra from 200 fs to 3.5 ns over the range 300 – 1000 nm reveal three common bands for the I- and G-AgC complexes (Figure 1). A band centered at 490 nm coincides with the steady-state absorption peak, and this negative band is assigned to ground state bleaching (GSB) that approaches the ΔA = 0 baseline with time (Figure 2). The positive absorption with λ_{max} of 660 nm is assigned to an excited state absorption because this absorption decays in lock step as the ground state recovers. This correlation suggests that this excited state directly feeds the ground state. Transient near-infrared absorption features have also been observed for other DNA-bound silver clusters.[37, 40] A negative-going band starts at 560 nm at 200 fs and shifts to 570 nm by 500 ps, and this band coincides with the steady-state emission band and is assigned to stimulated emission (Figure S1). While such emission has been observed for a NIR-emitting Ag_{20}–DNA conjugate at cryogenic temperatures,[41] it is reported here for the first time for a DNA-AgC in aqueous solution at room temperature. The emission appears promptly, so this early snapshot suggests that the emissive state is rapidly populated to develop most of the 2500 cm^{-1} Stokes shift within the ~200 fs IRF of

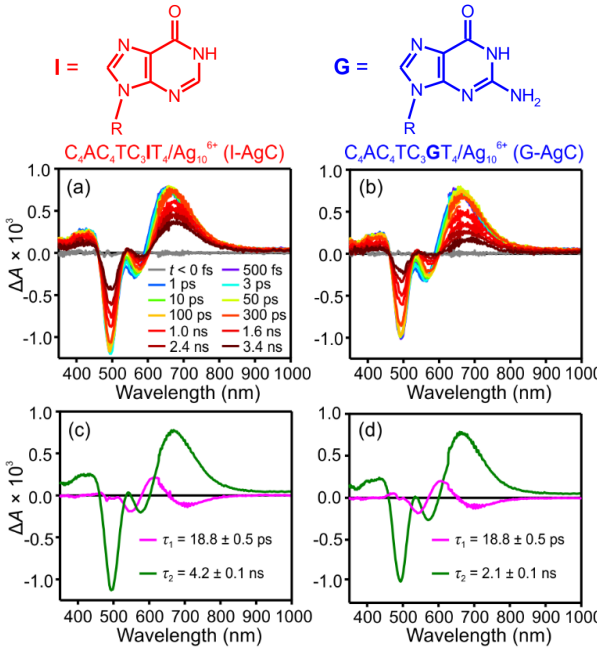

Figure 1. (a, b) Composite fs-TA spectra of I-AgC and G-AgC, respectively, recorded at selected delay times following 490 nm excitation. (c, d) Decay-associated difference spectra (DADS, see ref. 46) of I-AgC and G-AgC, respectively, obtained by globally fitting the TA data from 200 fs to 3.5 ns. Data were fit to a biexponential decay function $\Delta A(t) = A_1 \exp(-t/\tau_1) + A_2 \exp(-t/\tau_2)$. Uncertainties are re-

our spectrometer. Reveguk et al. attributed an ultrafast decay for their green-emitting DNA-AgC to a geometry change of the AgC core in the excited state.[42] The slow drift from 560 to 570 nm over its 500 ps range may be attributed to the flexibility of its host. DNA conformation fluctuations are sluggish in relation to solvation dynamics, as indicated by the ps and ns spectral shifts for DNA-bound red- and NIR-emitting silver clusters and DNA-intercalated organic dyes. [35, 38, 43-45]

Both the steady-state and transient spectra are similar for the two DNA-bound clusters, establishing that the two $C_4AC_4TC_3XT_4$ strands conserve the coordination site for their Ag_{10}^{6+} adducts. However, the two Ag_{10}^{6+} chromophores relax at different rates (Figure 2). When monitoring both the 490 nm GSB and the 660 nm ESA, the I-AgC complex returns to the ground state nearly monoexponentially with a 4.2 ± 0.1 ns lifetime. This decay time accounts for 97% of the ground state repopulation with the 3% balance of 18.8 ± 0.5 ps attributed to time-dependent shifts in the SE and ESA bands (Figure 1c). In contrast, the photoexcited G-AgC complex relaxes twice as rapidly with a 2.1 ± 0.2 ns time constant (98%) and an analogous 18.8 ± 0.5 ps component (2%) (Figure 1d). These transient absorption lifetimes match the amplitude-weighted fluorescence lifetimes (Table 1), independently supporting relaxation from the emissive excited state back to the ground state. We note that after approximately 100 ps the transient decays are monoexponential while the fluorescence decays are biexponential. The latter may result from monitoring the decay on the blue side of the fluorescence maximum, and/or the greater sensitivity and extended time window of the TCSPC vs. fs-TA measurements (200 ns vs 3.5 ns).[38, 43] The fs-TA data were also analyzed by fitting with an offset to look for decay pathways beyond our 3.5 ns limit (Figure S5 and Table S1 in the SI). The small offset amplitudes of 6% for I-AgC and 14% for G-AgC (Table S1) indicate that most of the fs-TA signal at 490 nm (GSB) decays on a nanosecond time scale, with G-AgC again decaying faster (2.3×) than I-AgC. More definitive evidence for a long-lived state is provided by ns-TA and fluorescence correlation measurements, which are described next.

2.2 Long Time Range

Nanosecond transient absorption (ns-TA) experiments show a GSB at 490 nm, and its kinetics were probed via two time windows - up to 1.6 μs with 0.2 ns resolution and up to 400 μs with 40 ns resolution. The shorter window shows a constant offset, thus substantiating the offset in our fs-TA fits (Figure 3a and S6). In our longer time window, this offset evolves into a bi-exponential decay with 20 μs (G-AgC)/25 μs (I-AgC) and ≳ 400 μs (G-AgC and I-AgC) lifetimes (Figure 3b). Such longer lifetimes of 1~100 μs have been observed for metastable states of other DNA-silver complexes.[37, 40, 47, 48]

The prompt ns-TA signals (t < 20 ns) are a convolution of not only the recovery of the ground state but also fluorescence from the emissive state. Furthermore, these decay faster than the 7.4 ns IRF. To address this limitation, we used the excitation conditions of the ns-TA experiments to estimate the initial GSB signal in our fs-TA experiments, and then comparing it to the amplitude of the long-lived state. This shows that roughly 4% of the excited-state population traps to the μs state for both I- and G-AgC (see Supplementary Material for full details). This quantum yield is consistent with studies of other DNA-bound clusters[37, 47, 49] and with the offsets in our ns-TA fits.

Fluorescence correlation spectroscopy independently supports a μs-lived state for the G-AgC complex. This technique monitors the fluctuations in the emission from a small number of molecules in a fL probe volume, and two components are resolved in the autocorrelation analysis (Figure S7). First, the emission fluctuates because the DNA-cluster complexes freely diffuse through the open, confocally-defined probe volume, and the time constant of ~260 μs is consistent with the hydrodynamic radii of DNA-silver cluster complexes.[39] The corresponding diffusion coefficient of 97 $\mu m^2/s$ and hydrodynamic volume of 45 nm^3 are consistent with earlier studies.[27] Second, the emission blinks if these fluorophores cross to a metastable dark electronic state, and the time constant of ~17 μs measured for G-AgC agrees with the decay time of 20 μs measured in the ns-TA experiment, thus further supporting shelving to a μs-lived electronic state (Figure 4b). [37]

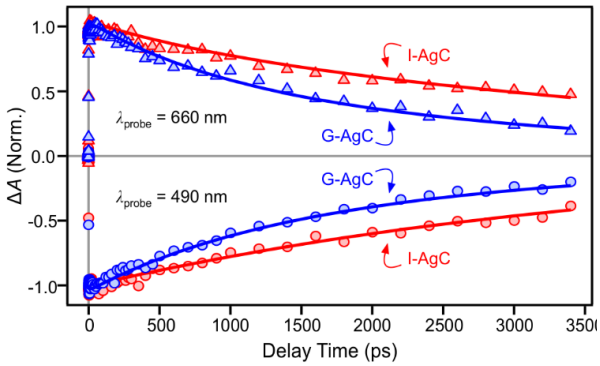

Figure 2. Kinetic decay traces of I-AgC (red) and G-AgC (blue) with probing at 490 nm (circles) and 660 nm (triangles) from 200 fs to 3.5 ns following 490-nm excitation. The markers are raw data and the solid traces are best-fit curves obtained from global fitting (see text). The traces have been normalized to the magnitude of the TA signal at 200 fs. The vertical and horizontal gray lines denote t = 0 and ΔA = 0, respectively.

2.3 Photophysical Model

Because photoexcited $C_4AC_4TC_3XT_4/Ag_{10}^{6+}$ complexes have a low dark state quantum yield of 4% (see SI) and because the fluorescence quantum yields of I-AgC and G-AgC are 63 and 25%, respectively, we propose that additional

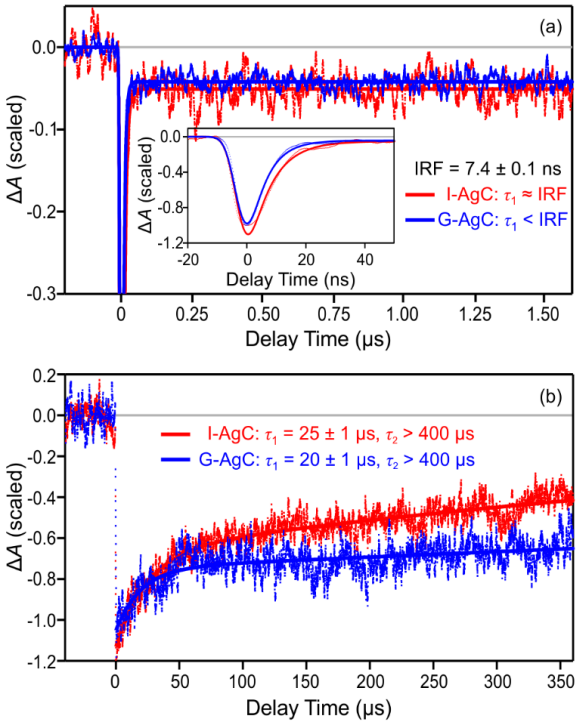

Figure 3. Normalized GSB kinetics of I-AgC (red) and G-AgC (blue) probed at 492 nm after 490 nm excitation, up to 1.6 μs with a step size of 0.2 ns (a), and up to 400 μs with a step size of 40 ns (b). The dots are the experimental data and the solid lines are best-fit curves. The curves in panel (a) were fit to a monoexponential decay function plus an offset, convoluted with a normalized Gaussian function: $\Delta A(t) = (A_1 \exp(-t/\tau_1) + A_2) * (1/(\sqrt{2\pi}\sigma) \exp(-t^2/(2\sigma^2))$. The curves in panel (b) were fit to a biexponential decay function $\Delta A(t) = A_1 \exp(-t/\tau_1) + A_2 \exp(-t/\tau_2)$. Uncertainties are reported as 2σ.

nonradiative relaxation from the fluorescent state competes with emission. This competition reveals the key distinction between the complexes (Table 1). While the radiative rates are similar, the nonradiative decay rate is nearly sevenfold higher for G-AgC than for I-AgC. The brightness and suppressed nonradiative decay rate of I-AgC could imply a weaker interaction between inosine and the metal cluster due to the missing C2-NH_2 group. The key question is whether this is a causative relationship, i.e. does DNA-cluster coordination control nonradiative relaxation? One possibility is that tight coordination facilitates orbital overlap that in turn promotes charge transfer and nonradiative relaxation.[50] Charge transfer and electron donation controls the electronic stability and photoluminescence of ligated noble-metal nanoclusters.[37, 51, 52] Mixed ligand and metal electronic states with charge transfer character have been proposed for atomically-precise silver clusters bound to thiolate ligands.[53, 54] A charge transfer state involving the ligand and the metal core is also predicted for DNA-AgC via theoretical calculations.[55, 56]

The metastable dark state is a minor sink following photoexcitation, but our fs-TA, ns-TA, and FCS studies indirectly identify this state because it hinders the ground state recovery. This state was further characterized by using aerated and deaerated solutions, and these yield identical signals in the 0-200 ns window of our ns-TA measurements (Figure S6). The absence of quenching by oxygen nominally argues against triplet states, but it is possible that the encapsulating DNA strands inhibit dissolved O_2 from reaching the cluster and quenching triplet states as seen when triplet emitters are encapsulated in cyclodextrins or other supramolecular structures.[35, 57]

IV. CONCLUSION

The two $C_4AC_4TC_3GT_4$-Ag_{10}^{6+} complexes with X = G and I are seemingly identical – the clusters have matching stoichiometries, oxidation states, and absorption/emission spectra. However, the guanosine strand is dimmer than the guanosine counterpart with a 2.5× lower fluorescence quantum yield and a 1.8× shorter fluorescence lifetime. While the two complexes have similar radiative lifetimes, the G-AgC cluster has a 7-fold more efficient nonradiative channel connecting the emissive state with the ground state in relation to the I-AgC cluster. Thus, the brightness of this DNA-AgC was modulated by a single-site mutation without compromising the structure of the cluster. Targeted changes to nucleobases that bind strongly to a given metal cluster suggest that cluster brightness can be tuned via the DNA scaffold.

SUPPLEMENTARY MATERIAL

See supplementary material for synthesis and characterization of the silver clusters, experimental methods for steady-state emission spectroscopy, broadband fs-TA, ns-TA and fluorescence correlation spectroscopy.

ACKNOWLEDGMENTS

Work at Ohio State University was supported by the U.S. National Science Foundation (CHE-1800471) and by funding from The Ohio State University. Work at Furman was supported by the National Science Foundation (CHE-1611451 and CHE-2002910) and the Furman Advantage program. This work was supported in part by the National Science Foundation EPSCoR Program under NSF Award No. OIA-1655740. This work was performed, in part, at the Center for Integrated Nanotechnologies, an Office of Science User Facility operated for the U.S. Department of Energy (DOE) Office of Science by Los Alamos National Laboratory (Contract 89233218CNA000001) and Sandia National Laboratories (Contract DE-NA-0003525).

DATA AVAILABILITY

The data that supports the findings of this study are available within the article and its supplementary material.

Table 1. The dominant decay component, τ_2, from fs-TA experiments, the amplitude-weighted emission lifetime, $\langle\tau\rangle$, and the estimated radiative lifetime, τ_r, and nonradiative lifetime, τ_{nr}, for the silver clusters studied.

	τ_2 (ns)[a]	$\langle\tau\rangle$ (ns)[b]	τ_r (ns)[c]	τ_{nr} (ns)[d]
I-AgC	4.2 ± 0.2	3.4 ± 0.1	5.4 ± 0.2	19 ± 5
G-AgC	2.1 ± 0.2	1.9 ± 0.3	7.6 ± 1.9	2.9 ± 0.5

[a] λ_{pump} = 490 nm.

[b] Amplitude-weighted lifetimes were calculated by $\langle\tau\rangle = \sum_i A_i\tau_i / \sum_i A_i$. Lifetimes and amplitudes are from fits to time-correlated single-photon counting (TCSPC) emission measurements with λ_{ex} = 470 nm, λ_{em} = 525 nm. Values are from Table 2 in Ref 27.

[c] Radiative lifetimes were calculated by $\tau_r = \langle\tau\rangle/Q_F$ using fluorescence quantum yield, Q_F, values from Table 2 in Ref 27.

[d] Time constants for nonradiative decay were calculated by $\tau_{nr}^{-1} = k_{nr} = \tau_2^{-1} - \tau_r^{-1}$.

REFERENCES

1. R. Kubo, Journal of the Physical Society of Japan **17** (6), 975-986 (1962).
2. R. Kubo, A. Kawabata and S.-I. Kobayashi, Annual Review of Materials Science **14** (1), 49-66 (1984).
3. J. Zheng, P. R. Nicovich and R. M. Dickson, Annual Review of Physical Chemistry **58**, 409-431 (2007).
4. W. Schulze, I. Rabin and G. Ertl, Chemphyschem **5** (3), 403-407 (2004).
5. C. I. Richards, S. Choi, J.-C. Hsiang, Y. Antoku, T. Vosch, A. Bongiorno, Y.-L. Tzeng and R. M. Dickson, Journal of the American Chemical Society **130** (15), 5038-5039 (2008).
6. S. M. Swasey, S. M. Copp, H. C. Nicholson, A. Gorovits, P. Bogdanov and E. G. Gwinn, Nanoscale **10** (42), 19701-19705 (2018).
7. H. C. Yeh, J. Sharma, J. J. Han, J. S. Martinez and J. H. Werner, Nano Lett **10** (8), 3106-3110 (2010).
8. J. T. Petty, O. O. Sergev, D. A. Nicholson, P. M. Goodwin, B. Giri and D. R. McMullan, Analytical Chemistry **85** (20), 9868-9876 (2013).
9. P. R. O'Neill, E. G. Gwinn and D. K. Fygenson, The Journal of Physical Chemistry C **115** (49), 24061-24066 (2011).
10. M. Brust, M. Walker, D. Bethell, D. J. Schiffrin and R. Whyman, Journal of the Chemical Society, Chemical Communications (7), 801-802 (1994).
11. S. Chen, R. S. Ingram, M. J. Hostetler, J. J. Pietron, R. W. Murray, T. G. Schaaff, J. T. Khoury, M. M. Alvarez and R. L. Whetten, Science **280** (5372), 2098-2101 (1998).
12. X. Kang and M. Zhu, Chemical Society Reviews **48** (8), 2422-2457 (2019).
13. Y. Li and R. Jin, Journal of the American Chemical Society **142** (32), 13627-13644 (2020).
14. H. Hakkinen, Nature Chemistry **4** (6), 443-455 (2012).
15. W. Hou, M. Dasog and R. W. J. Scott, Langmuir **25** (22), 12954-12961 (2009).
16. V. R. Jupally, R. Kota, E. V. Dornshuld, D. L. Mattern, G. S. Tschumper, D.-E. Jiang and A. Dass, Journal of the American Chemical Society **133** (50), 20258-20266 (2011).
17. A. Henglein, P. Mulvaney and T. Linnert, Faraday Discussions (92), 31-44 (1991).
18. J. Zheng and R. M. Dickson, Journal of the American Chemical Society **124** (47), 13982-13983 (2002).
19. T. Yamane and N. Davidson, Biochimica et Biophysica Acta **55**, 609-621 (1962).
20. M. Daune, C. A. Kekker and H. K. Schachman, Biopolymers **4**, 51-76 (1966).
21. J. T. Petty, J. Zheng, N. V. Hud and R. M. Dickson, Journal of the American Chemical Society **126** (16), 5207-5212 (2004).
22. C. M. Ritchie, K. R. Johnsen, J. R. Kiser, Y. Antoku, R. M. Dickson and J. T. Petty, Journal of Physical Chemistry C **111** (1), 175-181 (2007).
23. B. Sengupta, C. M. Ritchie, J. G. Buckman, K. R. Johnsen, P. M. Goodwin and J. T. Petty, Journal of Physical Chemistry C **112** (48), 18776-18782 (2008).
24. S. M. Copp, P. Bogdanov, M. Debord, A. Singh and E. Gwinn, Advanced Materials **26** (33), 5839-5845 (2014).
25. D. Schultz and E. G. Gwinn, Chemical Communications **48** (46), 5748-5750 (2012).
26. J. T. Petty, B. Giri, I. C. Miller, D. A. Nicholson, O. O. Sergev, T. M. Banks and S. P. Story, Analytical Chemistry **85** (4), 2183-2190 (2013).
27. J. T. Petty, M. Ganguly, A. I. Yunus, C. He, P. M. Goodwin, Y.-H. Lu and R. M. Dickson, The Journal of Physical Chemistry C **122** (49), 28382-28392 (2018).
28. J. T. Petty, O. O. Sergev, M. Ganguly, I. J. Rankine, D. M. Chevrier and P. Zhang, Journal of the American Chemical Society **138** (10), 3469-3477 (2016).

29. D. Schultz, K. Gardner, S. S. R. Oemrawsingh, N. Markeševic´, K. Olsson, M. Debord, D. Bouwmeester and E. Gwinn, Advanced Materials **25**, 2797-2803 (2013).
30. M. S. Blevins, D. Kim, C. M. Crittenden, S. Hong, H.-C. Yeh, J. T. Petty and J. S. Brodbelt, ACS Nano **13** (12), 14070-14079 (2019).
31. D. J. E. Huard, A. Demissie, D. Kim, D. Lewis, R. M. Dickson, J. T. Petty and R. L. Lieberman, Journal of the American Chemical Society **141** (29), 11465-11470 (2019).
32. C. Cerretani, H. Kanazawa, T. Vosch and J. Kondo, Angewandte Chemie - International Edition **58**, 17153 (2019).
33. R. R. Ramazanov, T. S. Sych, Z. V. Reveguk, D. A. Maksimov, A. A. Vdovichev and A. I. Kononov, The Journal of Physical Chemistry Letters **7** (18), 3560-3566 (2016).
34. D. Schultz, R. G. Brinson, N. Sari, J. A. Fagan, C. Bergonzo, N. J. Lin and J. P. Dunkers, Soft Matter **15** (21), 4284-4293 (2019).
35. A. Gonzàlez-Rosell, C. Cerretani, P. Mastracco, T. Vosch and S. M. Copp, Nanoscale Advances **3** (5), 1230-1260 (2021).
36. Y. Zhang, C. He, J. T. Petty and B. Kohler, The Journal of Physical Chemistry Letters **11** (21), 8958-8963 (2020).
37. S. A. Patel, M. Cozzuol, J. M. Hales, C. I. Richards, M. Sartin, J.-C. Hsiang, T. Vosch, J. W. Perry and R. M. Dickson, The Journal of Physical Chemistry C **113** (47), 20264-20270 (2009).
38. C. Cerretani, M. R. Carro-Temboury, S. Krause, S. A. Bogh and T. Vosch, Chem. Commun. **53** (93), 12556-12559 (2017).
39. C. He, P. M. Goodwin, A. I. Yunus, R. M. Dickson and J. T. Petty, The Journal of Physical Chemistry C **123** (28), 17588-17597 (2019).
40. J. T. Petty, C. Fan, S. P. Story, B. Sengupta, M. Sartin, J.-C. Hsiang, J. W. Perry and R. M. Dickson, The Journal of Physical Chemistry B **115** (24), 7996-8003 (2011).
41. E. Thyrhaug, S. A. Bogh, M. R. Carro-Temboury, C. S. Madsen, T. Vosch and D. Zigmantas, Nat. Commun. **8**, 15577 (2017).
42. Z. Reveguk, R. Lysenko, R. Ramazanov and A. Kononov, Phys. Chem. Chem. Phys. **20** (44), 28205-28210 (2018).
43. S. A. Bogh, M. R. Carro-Temboury, C. Cerretani, S. M. Swasey, S. M. Copp, E. G. Gwinn and T. Vosch, Methods and Applications in Fluorescence **6** (2), 024004 (2018).
44. D. Andreatta, J. L. Pérez Lustres, S. A. Kovalenko, N. P. Ernsting, C. J. Murphy, R. S. Coleman and M. A. Berg, Journal of the American Chemical Society **127** (20), 7270-7271 (2005).
45. R. Jimenez, G. R. Fleming, P. V. Kumar and M. Maroncelli, Nature **369** (6480), 471-473 (1994).
46. I. H. M. van Stokkum, D. S. Larsen and R. van Grondelle, Biochimica et Biophysica Acta (BBA) - Bioenergetics **1657** (2), 82-104 (2004).
47. T. Vosch, Y. Antoku, J.-C. Hsiang, C. I. Richards, J. I. Gonzalez and R. M. Dickson, Proceedings of the National Academy of Sciences of the United States of America **104** (31), 12616-12621 (2007).
48. J. T. Petty, C. Fan, S. P. Story, B. Sengupta, A. St. John Iyer, Z. Prudowsky and R. M. Dickson, The Journal of Physical Chemistry Letters **1** (17), 2524-2529 (2010).
49. I. L. Volkov, P. Y. Serdobintsev and A. I. Kononov, The Journal of Physical Chemistry C **117** (45), 24079-24083 (2013).
50. N. J. Turro, V. Ramamurthy and J. C. Scaiano., *Modern Molecular Photochemistry of Organic Molecules*. (Science Books, 2010).
51. Z. K. Wu and R. C. Jin, Nano Lett. **10** (7), 2568-2573 (2010).
52. M. Walter, J. Akola, O. Lopez-Acevedo, P. D. Jadzinsky, G. Calero, C. J. Ackerson, R. L. Whetten, H. Gronbeck and H. Häkkinen, Proceedings of the National Academy of Sciences of the United States of America **105** (27), 9157-9162 (2008).
53. M. Pelton, Y. Tang, O. M. Bakr and F. Stellacci, J. Am. Chem. Soc. **134** (29), 11856-11859 (2012).

54. S. H. Yau, B. A. Ashenfelter, A. Desireddy, A. P. Ashwell, O. Varnavski, G. C. Schatz, T. P. Bigioni and T. Goodson, J. Phys. Chem. C **121** (2), 1349-1361 (2017).
55. V. Soto-Verdugo, H. Metiu and E. Gwinn, J. Chem. Phys. **132** (19), 195102 (2010).
56. R. Longuinhos, A. D. Lúcio, H. Chacham and S. S. Alexandre, Physical Review E **93** (5), 052413 (2016).
57. M. A. Filatov, S. Baluschev and K. Landfester, Chem. Soc. Rev. **45** (17), 4668-4689 (2016).